The Astrophysical Journal Letters, 918:L8 (6pp), 2021 September 1 https://doi.org/10.3847/2041-8213/ac17ec

No Large Dependence of Planet Frequency on Galactocentric Distance

Naoki Koshimoto[1,2,3], David P. Bennett[1,2], Daisuke Suzuki[3], and Ian A. Bond[4]
[1] Laboratory for Exoplanets and Stellar Astrophysics, NASA/Goddard Space Flight Center, Greenbelt, MD 20771, USA
[2] Department of Astronomy, University of Maryland, College Park, MD 20742, USA
[3] Department of Earth and Space Science, Graduate School of Science, Osaka University, Toyonaka, Osaka 560-0043, Japan
[4] Institute of Information and Mathematical Sciences, Massey University, Private Bag 102-904, North Shore Mail Centre, Auckland, New Zealand
Received 2021 June 11; revised 2021 July 12; accepted 2021 July 27; published 2021 August 26

Abstract

Gravitational microlensing is currently the only technique that helps study the Galactic distribution of planets as a function of distance from the Galactic center. The Galactic location of a lens system can be uniquely determined only when at least two of the three quantities that determine the mass–distance relations are measured. However, even if only one mass–distance relation can be obtained, a large sample of microlensing events can be used to statistically discuss the Galactic distribution of the lenses. In this study, we extract the Galactic distribution of planetary systems from the distribution of the lens-source proper motion, $\mu_{\rm rel}$, for a given Einstein radius crossing time, $t_{\rm E}$, measured for the 28 planetary events in the statistical sample by Suzuki et al. Because microlensing is randomly caused by stars in our Galaxy, the observational distribution can be predicted using a Galactic model. We incorporate the planet-hosting probability, $P_{\rm host} \propto M_{\rm L}^{m} R_{\rm L}^{r}$, into a Galactic model for random-selected stars, where $M_{\rm L}$ is the lens mass ($\sim$host mass), and $R_{\rm L}$ is the Galactocentric distance. By comparing the observed distribution with the model-predicted $\mu_{\rm rel}$ distribution for a given $t_{\rm E}$ at various combinations of (m, r), we obtain an estimate $r = 0.2 \pm 0.4$ under a plausible uniform prior for m of $0 < m < 2$. This indicates that the dependence of the planet frequency on the Galactocentric distance is not large, and suggests that the Galactic bulge does have planets.

Unified Astronomy Thesaurus concepts: Exoplanets (498); Gravitational microlensing (672); Milky Way Galaxy (1054); Galactic bulge (2041)

1. Introduction

Although more than 3000 planetary systems have been discovered to date, most reside at distances <1 kpc from the Sun.[5] In this regard, gravitational microlensing is a unique technique because it is sensitive to planetary systems over a wide range of distances in our Galaxy, from the Galactic disk to the Galactic bulge (Gaudi 2012). Microlensing is currently the only technique capable of investigating the Galactic distribution of planets. However, no study measuring the distribution has yet been reported, mainly owing to the difficulty in distance measurement.

There are four physical quantities involved in each microlensing event: the lens mass $M_{\rm L}$, distance to the lens $D_{\rm L}$, distance to the source $D_{\rm S}$, and lens-source relative proper motion $\mu_{\rm rel}$—which is given by $\mu_{\rm rel} = |\mu_{\rm L} - \mu_{\rm S}|$, where $\mu_{\rm L}$ is the lens proper motion, and $\mu_{\rm S}$ is the source proper motion. For most planetary events, two parameters related to these quantities can be commonly measured via light curve modeling, i.e., the Einstein radius crossing time,

$$t_{\rm E} = \frac{\theta_{\rm E}}{\mu_{\rm rel}}, \tag{1}$$

and lens-source relative proper motion, $\mu_{\rm rel}$. Here, $\theta_{\rm E}$ is the angular Einstein radius given by

$$\theta_{\rm E} = \sqrt{\kappa M_{\rm L} \pi_{\rm rel}} \tag{2}$$

where $\kappa = 8.144$ mas $M_{\odot}^{-1}$ and $\pi_{\rm rel} = 1$ au$(D_{\rm L}^{-1} - D_{\rm S}^{-1})$.

Measuring either the microlens parallax or lens brightness, in addition to $t_{\rm E}$ and $\mu_{\rm rel}$, is required to determine $M_{\rm L}$ and $D_{\rm L}$, even assuming that the source star is located in the bulge (i.e., $D_{\rm S} \sim 8$ kpc). This requirement adds to the complexity of statistical studies focusing on determining the Galactic distribution of planets based on measured distances to the lens. The microlens parallax is measured only when the lens is relatively close to the Sun (Bennett et al. 2010). Because of the bias toward closer lenses and the vulnerability to systematic errors (Penny et al. 2016; Koshimoto & Bennett 2020), significant effort is required to prepare a clean statistical sample of a sufficient number of microlens parallax measurements.

Lens brightness measurements seem to be more robust in terms of susceptibility to systematic errors. However, to resolve the lens from the source, high-angular-resolution follow-up observations with adaptive optics or observations by the Hubble Space Telescope (HST) are required several years after the event. Thus, a certain amount of time is necessary to obtain a statistical sample of the lens brightness measurements. A systematic follow-up program for measuring the lens brightness for past planetary events is ongoing using the Keck telescope and HST (Bennett 2018; Bhattacharya et al. 2018), and a statistical sample of past planetary events with measurements of $t_{\rm E}$, $\mu_{\rm rel}$, and the lens brightness will be available in the near future.

Meanwhile, this study aims to extract information about the Galactic distribution of planets from a set of measurements of the Einstein radius crossing time, $t_{\rm E}$, and the lens-source relative proper motion $\mu_{\rm rel}$ for planetary events. Thus far, Penny et al. (2016) have attempted to compare the distance distribution of published microlensing planetary systems with predictions based on a Galactic model and proposed a possibility that the Galactic bulge might be devoid of planets. However, their results were affected by an inhomogeneous sample and incorrect microlens parallax measurements (Han et al. 2016).

[5] NASA Exoplanet Archive (https://exoplanetarchive.ipac.caltech.edu/; Akeson et al. 2013).

In this Letter, we compare the $\mu_{\rm rel}$ distribution for a given $t_{\rm E}$ of 28 planetary events from the statistical sample by Suzuki et al. (2016) with the distribution calculated using a Galactic model optimized for use in microlensing studies (Koshimoto & Ranc 2021; Koshimoto et al. 2021). We consider a power-law distribution, i.e., $P_{\rm host} \propto M_{\rm L}^{m} R_{\rm L}^{r}$, for the planet-hosting probability for lens stars, where $R_{\rm L}$ is the Galactocentric distance at which the lens is located. The comparison of the data and model for various (m, r) values enables us to estimate for the first time the dependence of the planet-hosting probability on the Galactocentric distance as $P_{\rm host} \propto R_{\rm L}^{0.2\pm0.4}$ when a uniform prior for m in $0 < m < 2$ is applied.

2. Method

This work aims to estimate the dependence of the planet-hosting probability on the Galactic location by comparing the $\mu_{\rm rel}$ distribution observed in planetary microlensing events with that predicted by a Galactic model. Although the microlens parallax and/or lens brightness have already been measured for some of the events in the sample, we here focus on the $t_{\rm E}$ and $\mu_{\rm rel}$ distributions to avoid any bias caused by including them. The $\mu_{\rm rel}$ distribution alone has no information about the lens mass, and little information about distance (Penny et al. 2016). However, when combined with $t_{\rm E}$, $\mu_{\rm rel}$ is equivalent to $\theta_{\rm E}$, which yields a mass–distance relation and allows us to extract mass and distance information.

Koshimoto & Bennett (2020) showed that an observed $\mu_{\rm rel}$ distribution can be compared with a model-expected distribution without considering a detection efficiency correction once $t_{\rm E}$ is fixed, i.e.,

$$f_{\rm obs}(\mu_{\rm rel}|t_{\rm E}) \propto \Gamma_{\rm Gal}(\mu_{\rm rel}|t_{\rm E}), \tag{3}$$

where $f_{\rm obs}(\mu_{\rm rel}|t_{\rm E})$ and $\Gamma_{\rm Gal}(\mu_{\rm rel}|t_{\rm E})$ are observed and expected $\mu_{\rm rel}$ distributions for given $t_{\rm E}$, respectively. $\Gamma_{\rm Gal}(\mu_{\rm rel}|t_{\rm E}) = \Gamma_{\rm Gal}(\mu_{\rm rel}, t_{\rm E})/\Gamma_{\rm Gal}(t_{\rm E})$, and $\Gamma_{\rm Gal}(\boldsymbol{x})$ is the microlensing event rate of events with parameter $\boldsymbol{x}$, which is calculated using the Galactic model explained in Section 4. The observed distribution is given by the sample described in Section 3.

A key idea behind Equation (3) is that the detection efficiency of a microlensing event depends on $t_{\rm E}$ but not on $\mu_{\rm rel}$; thus, detection efficiency calculations are not necessary to compare observations with simulations for a given $t_{\rm E}$. Technically, this is not true because the detection of a planetary signal in a light curve depends on the source radius crossing time, $t_* = \theta_*/\mu_{\rm rel}$, where θ_* is the angular source radius. However, this is expected to have little effect on our results because the dependence of the planet detection efficiency on t_* is negligibly small for a mass-ratio of $q \gtrsim 10^{-4}$ (Suzuki et al. 2016), which dominates our sample.

3. Planetary Microlensing Event Sample

We used 28 planetary microlensing events, which combine 22 planetary events detected by the MOA-II microlensing survey from 2007 to 2012 (Suzuki et al. 2016) and six planetary events from Gould et al. (2010) and Cassan et al. (2012). This is the same sample as the combined MOA+μFUN+PLANET sample in Suzuki et al. (2016), except for OGLE-2011-BLG-0950 (Choi et al. 2012). The event was excluded from our sample because both recent high-angular resolution imaging observations by S. K. Terry et al. (2021, in preparation) and the model-based prior probability calculation by Koshimoto et al. (2021) suggest that OGLE-2011-BLG-0950 was likely to be a stellar binary-lens event.

There are two events that have degenerate solutions with different $\mu_{\rm rel}$ values in the sample. MOA-2011-BLG-262 (Bennett et al. 2014) has the fast solution with $\mu_{\rm rel} = 19.6 \pm 1.6$ mas yr^{-1} and the slow solution with $\mu_{\rm rel} = 11.6 \pm 0.9$ mas yr^{-1}. We use only the slow solution in our analysis because it has a much larger prior probability as discussed in Bennett et al. (2014). MOA-2010-BLG-328 (Furusawa et al. 2013) has two parallax solutions ($u_0 < 0$ and $u_0 > 0$) and one xallarap solution, and the $\mu_{\rm rel}$ values are measured as 5.71 ± 0.70 mas yr^{-1}, 4.72 ± 0.79 mas yr^{-1}, and 4.03 ± 0.26 mas yr^{-1}, respectively. In the likelihood calculation described in Section 5, we equally combine the two parallax solutions, and then equally combine the combined parallax solution with the xallarap solution, i.e., we use $\sqrt{\mathcal{L}_{\rm xalla}\sqrt{\mathcal{L}_{\rm para+}\,\mathcal{L}_{\rm para-}}}$ as the likelihood for this event.

The black open circles in Figure 1 represent the $t_{\rm E}$ and $\mu_{\rm rel}$ values of the 28 planetary events; two of them, MOA-2007-BLG-192 (Bennett et al. 2008) and MOA-2011-BLG-322 (Shvartzvald et al. 2014), have only lower limit measurements on $\mu_{\rm rel}$. A more detailed description of Figure 1 is given in Section 5.

4. Galactic Model for Planet-hosting Stars

To calculate the model of the $\mu_{\rm rel}$ distribution for a given $t_{\rm E}$, $\Gamma_{\rm Gal}(\mu_{\rm rel}|t_{\rm E})$, we need a Galactic model for planet-hosting stars. This combines a model of planet-hosting probability, including the fit parameters investigated in this work, and a Galactic model for random-selected stars, which refers to a combination of the stellar mass function, stellar density distribution, and stellar velocity distribution in our Galaxy.

We consider that the planet-hosting probability for the lens depends on the lens mass $M_{\rm L}$ and Galactocentric distance $R_{\rm L}$ at which the lens is located, where Galactocentric distance refers to the radius in the cylindrical coordinate system with the Galactic center at the origin. The exact relation remains unknown; thus, in this study, a power law was adopted,

$$P_{\rm host}(M_{\rm L}, R_{\rm L}) \propto M_{\rm L}^{m} R_{\rm L}^{r}, \tag{4}$$

where m and r are the fit parameters for the powers of $M_{\rm L}$ and $R_{\rm L}$, respectively. Note that we used $P_{\rm host}(R_{\rm L}) = $ const. when $R_{\rm L} < 50$ pc to avoid singularity with $r < 0$. In the Appendix, we consider a dichotomous model for $P_{\rm host}(R_{\rm L})$ that does not have this singularity.

4.1. Galactic Model for Random-selected Stars

Koshimoto et al. (2021) developed a parametric Galactic model by fitting to Gaia Data Release 2 (DR2) velocity data (Gaia Collaboration et al. 2018), OGLE-III red clump star count data (Nataf et al. 2013), VIRAC proper motion data (Smith et al. 2018; Clarke et al. 2019), BRAVA radial velocity data (Rich et al. 2007; Kunder et al. 2012), and OGLE-IV star count and microlensing rate data (Mróz et al. 2017, 2019). All the data except for the Gaia DR2 data correspond to a bulge region of the sky, and the models are optimized for use in microlensing studies toward the Galactic bulge.

There are four versions of models developed in Koshimoto et al. (2021), which are denoted by E, G, E + E$_{\rm X}$, and G + G$_{\rm X}$. Each model consists of a multi-component thin disk, thick disk, and barred bulge. For the bulge density profile, exponential functions are used in the E and E + E$_{\rm X}$ models, whereas

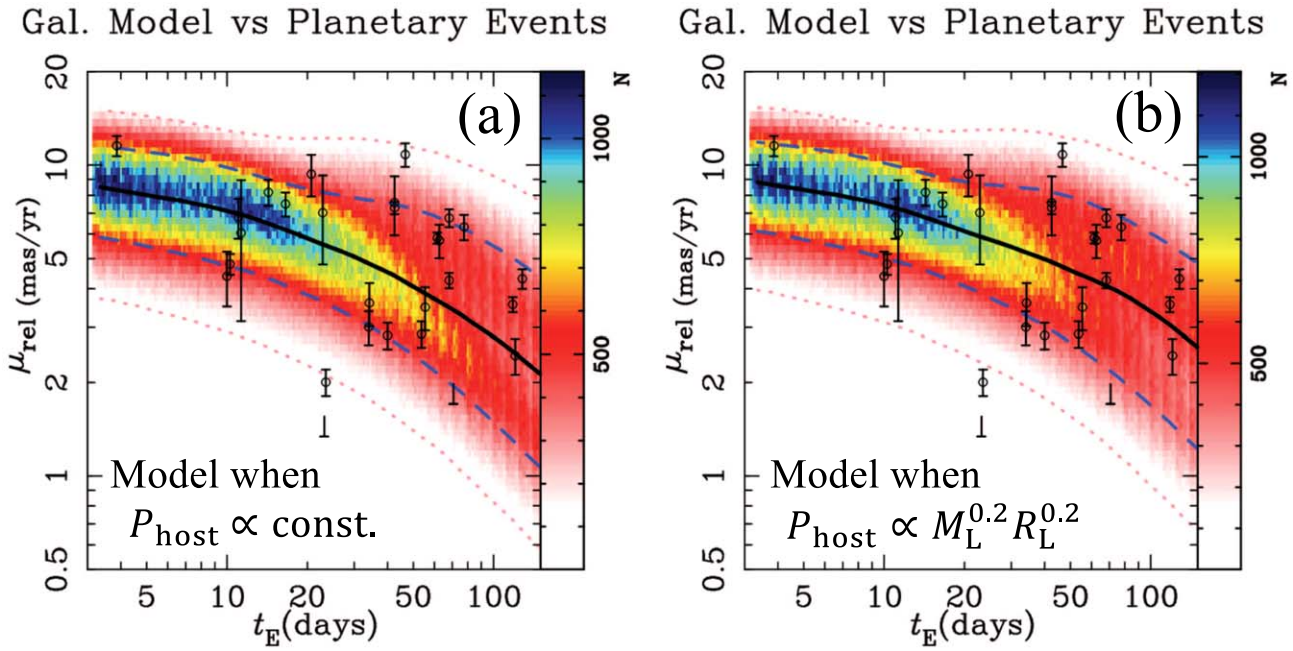

Figure 1. Comparison of the $\mu_{\rm rel}$ values of the 28 planetary events from the Suzuki et al. (2016) combined sample and Galactic model. The black open circles show the data, while the color map shows the model-calculated $\mu_{\rm rel}$ distribution for a given $t_{\rm E}$, $\Gamma_{\rm Gal}(\mu_{\rm rel}|t_{\rm E})$, as a function of fixed $t_{\rm E}$. The black solid, blue dashed, and magenta dotted lines indicate the median, 1σ, and 2σ for $\Gamma_{\rm Gal}(\mu_{\rm rel}|t_{\rm E})$, respectively. (a) Model with $P_{\rm host} \propto$ const, i.e., all stars are equally likely to host planets independent of their masses or locations in our Galaxy. (b) Model with $P_{\rm host} \propto M_{\rm L}^{0.2} R_{\rm L}^{0.2}$, corresponding to the best-fit grid that gives the maximum likelihood.

Gaussian functions are used in the G and $\rm G + G_X$ models. The E and G models have a single-component bulge density profile, whereas the $\rm E + E_X$ and $\rm G + G_X$ models have an additional component to represent the X-shape structure in the bulge (McWilliam & Zoccali 2010; Nataf et al. 2010). The different bulge profiles used in the four models led to different best-fit parameters for the stellar density, velocity, and initial mass function for all four models.

In this study, we used the $\rm E + E_X$ model as our fiducial Galactic model for random-selected stars because it was the most consistent with the data used in Koshimoto et al. (2021). We also used the other three models to evaluate the systematic errors in our measurement of the planet-hosting probability dependence.

4.2. Possibilities of Planets around White Dwarfs or Close-binaries

Our sample includes at least one circumbinary planet (OGLE-2007-BLG-349; Bennett et al. 2016). Because the number of events with lens brightness measurements in our sample is limited, there is a non-negligible chance that lens objects of other events may also consist of circumbinary planets or even planets around white dwarf hosts. Thus, both possibilities should be considered in the calculation of the event rate $\Gamma_{\rm Gal}(\mu_{\rm rel}|t_{\rm E})$.

We introduce two parameters to account for planet frequencies relative to single stars: $f_{\rm WD}$ for planets around white dwarfs and $f_{\rm CB}$ for planets around tight close-binaries. Values of $f_{\rm WD} = 1$ or $f_{\rm CB} = 1$ indicate the same planet frequency as for a single star with the same mass; if $f_{\rm WD} = 0$ or $f_{\rm CB} = 0$, there is zero probability of hosting planets. Determining the details of the planet abundance around white dwarfs or close-binary systems is beyond the scope of this study; thus, we adopted $(f_{\rm WD}, f_{\rm CB}) = (1, 1)$ for our fiducial model and used cases $(f_{\rm WD}, f_{\rm CB}) = (0, 1)$, $(1, 0)$, and $(0, 0)$ to evaluate the systematic errors in our r estimate.

To consider the white dwarf population and tight close-binary population in the model, we followed Koshimoto et al. (2021), where the initial-final mass relation of $M_{\rm WD} = 0.109 M_{\rm ini} + 0.394 M_\odot$ (Kalirai et al. 2008) is used for the white dwarfs. Further, the binary distribution developed by Koshimoto et al. (2020), together with a detection threshold based on a combination of the central caustic size of a hypothetical binary and the event impact parameter u_0, are used for tight close-binaries.

We assume that the planet-hosting probability for a neutron star or black hole is zero. The assumption is based on the study by Behrens et al. (2020) that found no planets in an 11 yr data set for 45 pulsars. If this rareness of planets around neutron stars is attributed to the progenitor's explosion (i.e., supernova), planets are also likely to be rare around black holes.

5. Maximum Likelihood Analysis

The color maps in Figure 1 are two examples of the model-calculated $\mu_{\rm rel}$ distribution for given $t_{\rm E}$, $\Gamma_{\rm Gal}(\mu_{\rm rel}|t_{\rm E})$, $(m,\ r) = (0,\ 0)$ in Figure 1(a) and $(m,\ r) = (0.2,\ 0.2)$ in Figure 1(b). The distributions are calculated over the range $0.50 < \log(t_{\rm E}/{\rm days}) < 2.20$. First, this range is divided into 34 bins of width 0.05 dex each. Then, 10^5 artificial events are generated using our fiducial Galactic model for planet-hosting stars, i.e., the $\rm E + E_X$ model with $(f_{\rm WD}, f_{\rm CB}) = (1,\ 1)$. We selected a Galactic coordinate of $(l, b) = (1.^\circ 0, -2.^\circ 2)$ for these plots. The coordinates of each event are used in the relative likelihood calculations presented below.

Figure 1(a) shows that the observed $\mu_{\rm rel}$ distribution is already in good agreement with the model, in which no planet-hosting probability dependence on the stellar mass or position in our Galaxy is assumed. This means that $(m, r) = (0, 0)$ is an acceptable planet-hosting probability dependence under the current constraint imposed by the data. Below, we calculate the

relative likelihood for various combinations of (m, r) and obtain the probability distributions for these parameters.

5.1. Definition of Likelihood

We define the likelihood for a combination of m and r as

$$\mathcal{L}(m, r) = \prod_i \Gamma_{\rm Gal}(\mu_{{\rm rel},i}|t_{{\rm E},i}; m, r), \quad (5)$$

where $\mu_{{\rm rel},i}$ and $t_{{\rm E},i}$ are the ones observed for ith event, and $\Gamma_{\rm Gal}(\mu_{{\rm rel},i}|t_{{\rm E},i}; m, r)$ is the model-calculated probability of $\mu_{{\rm rel},i}$ for given $t_{{\rm E},i}$ when the planet-hosting probability is $P_{\rm host} \propto M_{\rm L}^m R_{\rm L}^r$. The product is taken over all 28 events in our sample.

For each event i, in the calculation of $\Gamma_{\rm Gal}(\mu_{{\rm rel},i}|t_{{\rm E},i}; m, r)$, the corresponding parameters are used, e.g., the Galactic coordinate and impact parameter u_0 affecting the close-binary possibilities.

5.2. Results

We calculated the likelihood given by Equation (5) over the ranges of $-2 < m < 2$ and $-2 < r < 2$ at intervals of 0.2, for both m and r. This corresponds to applying uniform prior distributions for the two parameters between -2 and 2, which reflects that there are moderate fractions of planets in all categories of low-mass lenses (e.g., MOA-2008-BLG-310, Janczak et al. 2010; Bhattacharya et al. 2017; Koshimoto et al. 2020), high-mass lens (e.g., OGLE-2012-BLG-0026, Han et al. 2013; Beaulieu et al. 2016), distant lens (e.g., MOA-2007-BLG-400, Dong et al. 2009; Bhattacharya et al. 2021), and close lens (e.g., OGLE-2006-BLG-109, Gaudi et al. 2008; Bennett et al. 2010). The planet frequency dependence on $M_{\rm L}$ or $R_{\rm L}$ would not be as extreme as $|m| > 2$ or $|r| > 2$.

Figure 2 shows the results, where a clear negative correlation between m and r is seen. The shape of the correlation is attributed to the mass–distance relation given by the angular Einstein radius $\theta_{\rm E}$, a parameter equivalent to $\mu_{\rm rel}$ for a given $t_{\rm E}$. Because certain $\theta_{\rm E}$ values can be explained by both a low-mass lens close to the Sun and a high-mass lens close to the source, the data distribution can be reproduced by both small m with large r and large m with small r. This degeneracy can be disentangled by including observational information of either the microlens parallax, lens brightness, or Einstein radius crossing time $t_{\rm E}$ with a proper detection efficiency correction, which all are interesting future works.

On the other hand, the location of the negatively correlated distribution on the r versus m plane is determined by the data and Galactic model. Figure 2 shows a high likelihood value at $(m, r) = (0, 0)$, as expected from Figure 1(a). For comparison, we show the $\Gamma_{\rm Gal}(\mu_{\rm rel}|t_{\rm E})$ distribution using the best-fit grid value of $(m, r) = (0.2, 0.2)$ in Figure 1(b). The correlation between r and m becomes weaker when m increases, and a stronger constraint can be placed on r than m, for which we have estimated $r = 0.4^{+0.6}_{-0.4}$.

Because it is difficult to put a useful constraint on the m value based on the current data, we considered a stronger uniform prior on m in the range $0 < m < 2$. This is a plausible prior considering the ongoing high-angular resolution follow-up program on past events (Bennett 2018), which revealed that two events (out of seven published) have lens host stars that are much more massive than those expected by Bayesian analysis using a Galactic model for random-selected stars (Vandorou et al. 2020; Bhattacharya et al. 2021).[6] For giant planets, the possibility of $m > 0$ is also supported by other techniques. Johnson et al. (2010) estimated $m = 1.0 \pm 0.3$ in $\lesssim$2.5 au from a radial velocity survey, and Nielsen et al. (2019) estimated $m = 2.0 \pm 1.0$ in 10–100 au from a direct imaging survey.

As shown by the red dotted curve in the top panel of Figure 2, applying the narrower prior of $0 < m < 2$ can almost entirely exclude the possibility of $r > 1$. The median and 1σ error is $r = 0.2 \pm 0.4$ for the fiducial E + E_X Galactic model with $(f_{\rm WD}, f_{\rm CB}) = (1, 1)$.

Finally, to evaluate the systematic error due to model selection, we repeated this analysis using the E, G, and G + G_X models and for $(f_{\rm WD}, f_{\rm CB}) = (1, 0)$, $(0, 1)$, and $(0, 0)$. We found that the median value of r becomes 0.3–0.5 and 0.2–0.3 for the

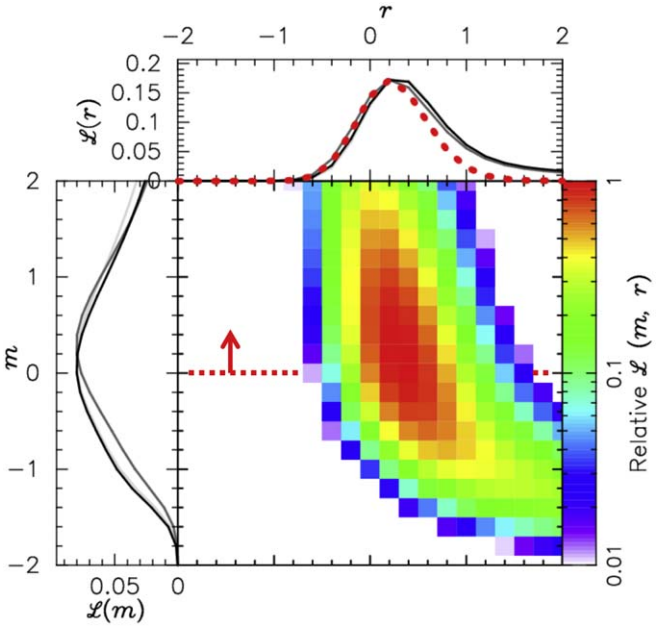

Figure 2. Relative likelihood distribution as a function of m and r for the E + E_X fiducial Galactic model with $(f_{\rm WD}, f_{\rm CB}) = (1, 1)$. In the top panel, probability distributions of r are shown in solid black and dotted red, integrated $\mathcal{L}(m, r)$ over $-2 < m < 2$ and $0 < m < 2$, respectively. The dark and light gray lines in the edge panels are the marginalized probability distributions when $(f_{\rm WD}, f_{\rm CB}) = (0, 1)$ and $(f_{\rm WD}, f_{\rm CB}) = (1, 0)$, respectively. (Note that the light gray line almost overlaps with the black line.)

Table 1
Results of the Maximum Likelihood Analysis

Range of Uniform Prior	r		m[c]
	Fiducial[a]	Sys. Range[b]	Fiducial[a]
$-2 < m < 2$	$0.4^{+0.6}_{-0.4}$	0.3–0.5	0.2 ± 1.0
$0 < m < 2$	0.2 ± 0.4	0.2–0.3	$0.7^{+0.8}_{-0.6}$

Notes.
[a] Median and 1σ error for the E + E_X model and $(f_{\rm WD}, f_{\rm CB}) = (1, 1)$.
[b] Variation of median values when other Galactic models or other combinations of $(f_{\rm WD}, f_{\rm CB})$ are applied.
[c] Listed for completeness. The estimates of m are dominated by the prior applied.

[6] Our preliminary result from a statistical study on the Suzuki et al. (2016) sample based on mass measurements implies $m > 0$ with a 3σ confidence level, as reported by DPB in the Exoplanet Demographics Conference in November 2020. The talk can be found on https://www.youtube.com/watch?v=5TpOKjHSS10.

uniform priors in $-2 < m < 2$ and $0 < m < 2$, respectively. Thus, the systematic errors seem to be much smaller than the statistical errors. Table 1 summarizes the results of our likelihood analysis.

6. Discussion and Conclusion

We estimated the planet-hosting probability dependence of $P_{\rm host} \propto R_{\rm L}^{0.2\pm0.4}$ under a uniform prior distribution of m in $0 < m < 2$, which suggests no large dependence of the planet frequency on the Galactocentric distance. The bulge region has a very different stellar environment from the solar neighborhood, including stellar densities $\gtrsim$10 times higher and an older, alpha-enhanced stellar population. Observations of the solar neighborhood have shown that there is a correlation between stellar metallicity and the occurrence of giant planets (Fischer & Valenti 2005; Johnson et al. 2010), and have also suggested that close encounters with other stars may affect the evolution of planetary systems (Winter et al. 2020). Therefore, due to the abovementioned environmental differences, the planet frequency in the bulge may differ significantly from that in the solar neighborhood. Although our results are still inconclusive, they might imply that cold planets orbiting beyond the H_2O snow line also commonly exist in the bulge region regardless of such differences.

Because all exoplanet detection techniques have sensitivities that complement each other, it is important to combine different techniques for a comprehensive understanding of planet formation and evolution processes (Gaudi et al. 2020). One of the largest uncertainties when comparing the exoplanet population discovered via other exoplanet detection methods with microlensing planets is a possible large dependence of the planet frequency on Galactic location. Our results show that such a dependence is not very large, and one might be able to compare them without considering the difference in Galactic location. A small dependence of the planet frequency on the Galactic location is also supported by Suzuki et al. (2016). Suzuki et al. (2016) showed that the planet frequency from the MOA-II microlensing survey—which is an averaged value for stars in the galactic disk and bulge—is consistent with the frequency of cold gas giants from radial velocity studies (Bonfils et al. 2013; Montet et al. 2014).

On the other hand, the full consistency with $r = 0$ contrasts with the analysis by Penny et al. (2016), who found a small p-value of 5.0×10^{-4} for a model in which the planetary frequency of the bulge is the same as that of the disk. The difference is most likely due to the contamination of excessively close lenses with incorrect parallax measurements in their sample. Penny et al. (2016) discussed this possibility, and questioned the results of several events with large microlens parallax values. In fact, among the questioned events, OGLE-2013-BLG-0723 was a stellar binary event (Han et al. 2016). The large microlens parallax claimed for MOA-2007-BLG-192 (Bennett et al. 2008) has recently been shown to disappear when the data are detrended for color-dependent differential refraction (Bennett et al. 2012), although this has not yet been published. Nevertheless, our results are still consistent with the Penny et al. (2016)'s estimate of the bulge-to-disk ratio of planet frequency, $f_{\rm bulge} < 0.54$, as shown in the Appendix.

Our estimate of $r = 0.2 \pm 0.4$ still has a moderately large uncertainty, and there could be a non-negligible dependence of planet frequency on the Galactocentric distance $R_{\rm L}$. In particular, although $m > 0$ seems to be thus far plausible (Vandorou et al. 2020; Bhattacharya et al. 2021), if the possibility of $m < 0$ is considered, the uncertainty and preference for disk planets could increase. This is owing to the negative correlation between m and r, as shown in Figure 2, which is attributed to our use of only one parameter (i.e., $\theta_{\rm E}$) that provides a lens mass–distance relation in the analysis. Thus, further constraints should emerge by including constraints from other mass–distance relations, which can be provided by a statistical sample of either microlens parallax or lens brightness measurements.

N.K. was supported by the JSPS overseas research fellowship. D.P.B. and N.K. were supported by NASA through grant NASA-80NSSC18K0274 and award number 80GSFC17M0002. D.S. was supported by JSPS KAKENHI grant No. JP19KK082 and JP20H04754.

Appendix
Dichotomous Model for Planet-hosting Probability

One might think that the power-law model, $P_{\rm host} \propto R_{\rm L}^{r}$, is not physical because it diverges at $R_{\rm L} = 0$ when $r < 0$. Here, we consider a dichotomous model for the dependence of the planet-hosting probability on the lens Galactic location,

$$P_{\rm host}(R_{\rm L}) = \begin{cases} P_{\rm host,D} & \text{when } R_{\rm L} > 2 \text{ kpc} \\ P_{\rm host,B} & \text{when } R_{\rm L} \leqslant 2 \text{ kpc}, \end{cases} \quad \text{(A1)}$$

and we use the ratio between the two constants, $f_{\rm B/D} \equiv P_{\rm host,B}/P_{\rm host,D}$, as the fit parameter instead of r. This is a more directly comparable model to that used by Penny et al. (2016), who considered the bulge-to-disk ratio of planet frequency in the Han & Gould (2003) Galactic model, $f_{\rm bulge}$. Note that there is still a subtle difference between the two parameters—$f_{\rm B/D} = 0$ indicates that there are no planets at $R_{\rm L} \leqslant 2$kpc, whereas $f_{\rm bulge} = 0$ allows planet-hosting stars in the disk component to exist at $R_{\rm L} \leqslant 2$ kpc.

Figure 3 and Table 2 show the results of the maximum likelihood analysis using $f_{\rm B/D}$ instead of r, where the uniform

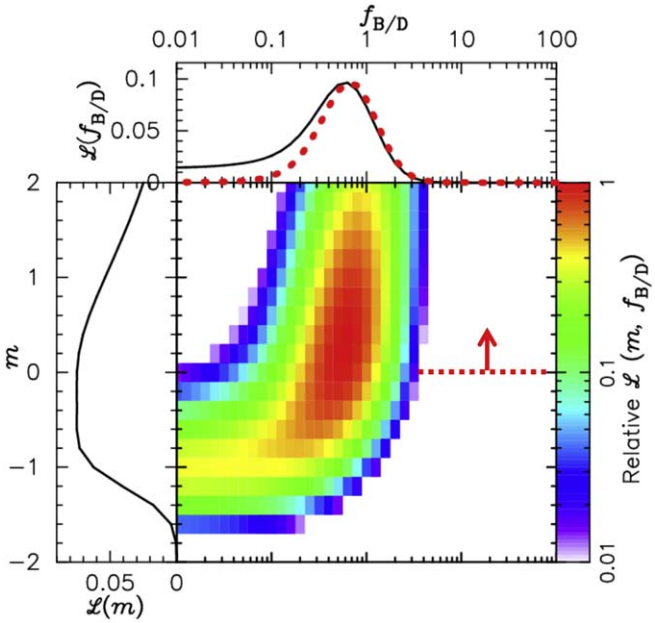

Figure 3. Same as Figure 2, but for $f_{\rm B/D}$ instead of r.

Table 2
$f_{B/D}$ Estimated from the Maximum Likelihood Analysis

Range of Uniform Prior	$f_{B/D}$	
	Fiducial[a]	Sys. Range[b]
$-2 < m < 2$	$0.48^{+0.59}_{-0.33}$	0.42–0.52
$0 < m < 2$	$0.63^{+0.61}_{-0.33}$	0.56–0.65

Notes.
[a] Median and 1σ error with the E + E_X model and $(f_{WD}, f_{CB}) = (1, 1)$.
[b] Variation of median values when other Galactic models or other combinations of (f_{WD}, f_{CB}) are applied.

prior for $\log f_{B/D}$ in $-2 < \log f_{B/D} < 2$ is assumed. With the uniform prior for m in $0 < m < 2$, we estimate $f_{B/D} = 0.63^{+0.61}_{-0.33}$, which is consistent with both $f_{B/D} = 1$ and $f_{bulge} < 0.54$; the upper limit estimate for f_{bulge} was taken from a p-value threshold of 0.01 by Penny et al. (2016).

ORCID iDs

Naoki Koshimoto https://orcid.org/0000-0003-2302-9562
David P. Bennett https://orcid.org/0000-0001-8043-8413
Daisuke Suzuki https://orcid.org/0000-0002-5843-9433

References

Akeson, R. L., Chen, X., Ciardi, D., et al. 2013, PASP, 125, 989
Beaulieu, J.-P., Bennett, D. P., Batista, V., et al. 2016, ApJ, 824, 83
Behrens, E. A., Ransom, S. M., Madison, D. R., et al. 2020, ApJL, 893, L8
Bennett, D. 2018, Keck Observatory Archive, N139, 172
Bennett, D. P., Batista, V., Bond, I. A., et al. 2014, ApJ, 785, 155
Bennett, D. P., Bond, I. A., Udalski, A., et al. 2008, ApJ, 684, 663
Bennett, D. P., Rhie, S. H., Nikolaev, S., et al. 2010, ApJ, 713, 837
Bennett, D. P., Rhie, S. H., Udalski, A., et al. 2016, AJ, 152, 125
Bennett, D. P., Sumi, T., Bond, I. A., et al. 2012, ApJ, 757, 119
Bhattacharya, A., Beaulieu, J.-P., Bennett, D. P., et al. 2018, AJ, 156, 289
Bhattacharya, A., Bennett, D. P., Anderson, J., et al. 2017, AJ, 154, 59
Bhattacharya, A., Bennett, D. P., Beaulieu, J. P., et al. 2021, AJ, 162, 60
Bonfils, X., Delfosse, X., Udry, S., et al. 2013, A&A, 549, A109
Cassan, A., Kubas, D., Beaulieu, J.-P., et al. 2012, Natur, 481, 167
Choi, J.-Y., Shin, I.-G., Han, C., et al. 2012, ApJ, 756, 48
Clarke, J. P., Wegg, C., Gerhard, O., et al. 2019, MNRAS, 489, 3519
Dong, S., Bond, I. A., Gould, A., et al. 2009, ApJ, 698, 1826
Fischer, D. A., & Valenti, J. 2005, ApJ, 622, 1102
Furusawa, K., Udalski, A., Sumi, T., et al. 2013, ApJ, 779, 91
Gaia Collaboration, Katz, D., Antoja, T., et al. 2018, A&A, 616, A11
Gaudi, B. S. 2012, ARA&A, 50, 411
Gaudi, B. S., Bennett, D. P., Udalski, A., et al. 2008, Sci, 319, 927
Gaudi, B. S., Christiansen, J. L., & Meyer, M. R. 2020, arXiv:2011.04703
Gould, A., Dong, S., Gaudi, B. S., et al. 2010, ApJ, 720, 1073
Han, C., Bennett, D. P., Udalski, A., et al. 2016, ApJ, 825, 8
Han, C., & Gould, A. 2003, ApJ, 592, 172
Han, C., Udalski, A., Choi, J.-Y., et al. 2013, ApJL, 762, L28
Janczak, J., Fukui, A., Dong, S., et al. 2010, ApJ, 711, 731
Johnson, J. A., Aller, K. M., Howard, A. W., et al. 2010, PASP, 122, 905
Kalirai, J. S., Hansen, B. M. S., Kelson, D. D., et al. 2008, ApJ, 676, 594
Koshimoto, N., Baba, J., & Bennett, D. P. 2021, ApJ, in press (arXiv:2104.03306)
Koshimoto, N., & Ranc, C. 2021, nkoshimoto/genulens v1.1: A Tool for Gravitational Microlensing Events Simulation, Zenodo, doi:10.5281/zenodo.4784948
Koshimoto, N., & Bennett, D. P. 2020, AJ, 160, 177
Koshimoto, N., Bennett, D. P., & Suzuki, D. 2020, AJ, 159, 268
Kunder, A., Koch, A., Rich, R. M., et al. 2012, AJ, 143, 57
McWilliam, A., & Zoccali, M. 2010, ApJ, 724, 1491
Montet, B. T., Crepp, J. R., Johnson, J. A., et al. 2014, ApJ, 781, 28
Mróz, P., Udalski, A., Skowron, J., et al. 2017, Natur, 548, 183
Mróz, P., Udalski, A., Skowron, J., et al. 2019, ApJS, 244, 29
Nataf, D. M., Gould, A., Fouqué, P., et al. 2013, ApJ, 769, 88
Nataf, D. M., Udalski, A., Gould, A., et al. 2010, ApJL, 721, L28
Nielsen, E. L., De Rosa, R. J., Macintosh, B., et al. 2019, AJ, 158, 13
Penny, M. T., Henderson, C. B., & Clanton, C. 2016, ApJ, 830, 150
Rich, R. M., Reitzel, D. B., Howard, C. D., et al. 2007, ApJL, 658, L29
Shvartzvald, Y., Maoz, D., Kaspi, S., et al. 2014, MNRAS, 439, 604
Smith, L. C., Lucas, P. W., Kurtev, R., et al. 2018, MNRAS, 474, 1826
Suzuki, D., Bennett, D. P., Sumi, T., et al. 2016, ApJ, 833, 145
Vandorou, A., Bennett, D. P., Beaulieu, J.-P., et al. 2020, AJ, 160, 121
Winter, A. J., Kruijssen, J. M. D., Longmore, S. N., et al. 2020, Natur, 586, 528